Structure and Dynamics in Columnar Discotic Materials: A Combined X-ray and Solid-State NMR Study of Hexabenzocoronene Derivatives

Ingrid Fischbach, Tadeusz Pakula, Piotr Minkin, Andreas Fechtenkötter, Klaus Müllen, and Hans Wolfgang Spiess*

Max-Planck-Institute for Polymer Research, Ackermannweg 10, D-55128 Mainz, Germany

Kay Saalwächter

Institut für Makromolekulare Chemie, Universität Freiburg, Stefan-Meier-Strasse 31, D-70104, Freiburg, Germany

Received: January 28, 2002; In Final Form: April 8, 2002

The solid columnar discotic and liquid crystalline (LC) phases formed by alkyl-substituted hexabenzocoronene (HBC) mesogens have been investigated by a combination of X-ray scattering and a variety of advanced solid-state NMR methods. Correlations between chemical structure, molecular packing and dynamics are established. Maximum charge carrier mobility is observed for a crystal-like stacking of the disks in the column with optimized $\pi-\pi$ interactions. For systems with lower intracolumnar order the charge carrier mobility is slightly lower and slow axial motion of the disks around the column axes occurs.

Introduction

An important issue in materials science is the understanding of a material's macroscopic properties on a molecular level. A class of organic solids of particular interest are conducting discotic liquid crystalline materials, such as the well-known triphenylenes. These materials might serve as active electronic components in future devices.[1−4] X-ray scattering and nuclear magnetic resonance are powerful and complementary tools for the investigation of structure and dynamics in organic solids,[5−7] and have already been successfully applied to the investigation of various discotic liquid crystalline materials (ref 8 and references therein).

We apply modern NMR methods and wide-angle X-ray scattering to the investigation of alkyl substituted hexabenzocoronenes, which have a number of favorable properties compared to the more established triphenylenes; for example they exhibit unusually large liquid crystalline phase widths and favorable physical and optoelectronic properties.[9] In this study, we continue and extend our previous work[10,11] on two columnar discotic derivatives of hexabenzocoronene (**1**), the dodecyl substituted HBC−C_{12} (**2**), and the dodecylphenyl-substituted HBC−PhC_{12} (**3**). This work focuses on the comparison of the yet uninvestigated behavior in the room-temperature phases of these materials with the behavior in the high-temperature LC phases.

Both HBC−C_{12} and HBC−PhC_{12} exhibit very high one-dimensional charge carrier mobilities (>1 $cm^2\ V^{-1}\ s^{-1}$ in the solid phases), which are already approaching the value for the intersheet mobility in graphite (3 $cm^2\ V^{-1}\ s^{-1}$).[12] It was recently shown that HBC−PhC_{12} could be successfully employed as an active medium for charge transport in a photovoltaic device operating at room temperature.[1]

As can be seen in the DSC traces (Figure 1), both HBC−C_{12} and HBC−PhC_{12} form hexagonal discotic mesophases above

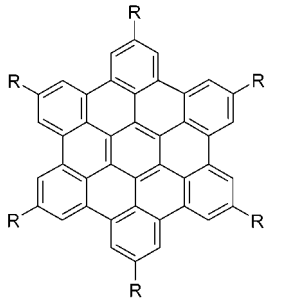

1 R = H **2** R = *n*-$C_{12}H_{25}$

3 R = 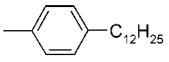 $C_{12}H_{25}$

107 °C and 80 °C, respectively. From previous investigations it is known that the disks undergo fast rotation in the columnar LC phases.[9−11] Upon entering the LC phase of HBC−C_{12}, the intracolumnar charge carrier mobility drops to about 0.3 $cm^2\ V^{-1}\ s^{-1}$.[12] On the contrary, no decrease of conductivity is observed for HBC−PhC_{12}. Rather, the conductivity remains almost constant over the whole temperature range, with a trend toward higher mobilities at higher temperatures and a mean value of about 0.3 $cm^2\ V^{-1}\ s^{-1}$. The question that arises concerns the molecular origin of these different behaviors.

Previous comparisons[13] of experimental ^1H double quantum spectra with ab initio simulated spectra for different molecular packing arrangements revealed that HBC−C_{12} forms a so-called herringbone packing arrangement in its room-temperature phase. This arrangement also accounts for the observation of three distinct aromatic ^1H resonances, which are π-shifted up to 3 ppm from the solution chemical shift.[10] The optimized $\pi-\pi$ overlap of the aromatic cores in such an arrangement accounts for the observed high charge carrier mobilities. In the LC phase the ^1H resonance lines are averaged due to the axial motion of the disks. The pronounced π-shift of this averaged line shows that the relative displacement of adjacent disks in the columns must be similar to the herringbone structure.[10,13] Since charge

* To whom correspondence should be addressed. E-mail: spiess@mpip-mainz.mpg.de.

10.1021/jp0255684 CCC: $22.00
Published on Web 05/25/2002

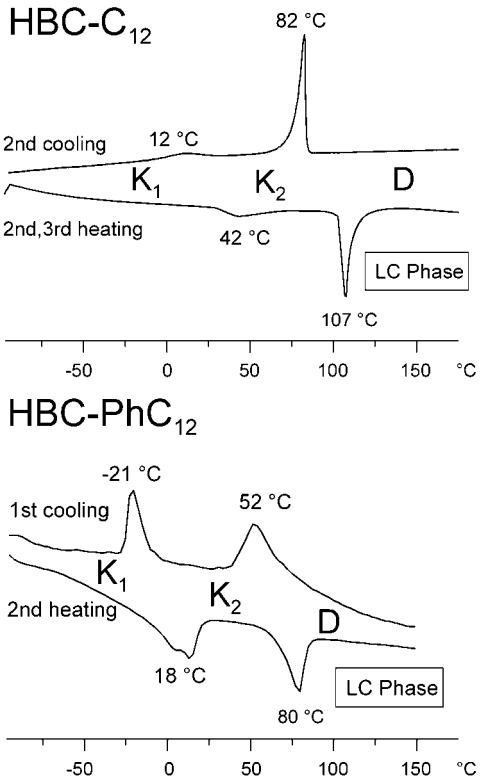

Figure 1. DSC-traces of HBC−C_{12} and HBC−PhC_{12}. The phase transition temperatures are given above the respective peaks.

transport occurs on a much faster time scale than the disk rotation, the increased mobility alone cannot explain the observed drop in conductivity upon entering the LC phase. The drop in the charge carrier mobility is most probably due to a loss of crystalline order.

The insertion of a phenyl-ring into the side chain undermines the crystal-like optimized $\pi-\pi$ packing, which is shown by the fact that HBC−PhC_{12} does not form such a highly ordered herringbone packing arrangement: this will be shown in this paper by heteronuclear correlation (HETCOR) NMR and 2D-WAXS (2D = two-dimensional).

Previously uninvestigated are slow dynamic processes in the HBCs. Such processes could contribute to self-healing processes in the column packing, which is highly desirable since the electronic properties in such systems are limited by the degree of long-range order within the columns. Our method of choice to investigate the slow dynamic processes on a molecular level is the relatively new one-dimensional (1D) CODEX (centerband-only detection of exchange) experiment,[14] which will be shortly described later and is described in great detail in ref 15.

Here we present the results of the CODEX measurements on the HBCs. For the evaluation of the CODEX data we determined the required ^{13}C−CSA tensor values by the SUPER (separation of undistorted powder-patterns by effortless recoupling) experiment introduced very recently by Schmidt-Rohr and co-workers.[16] This experiment allows the acquisition of quasi-static powder patterns in the indirect dimension of a 2D ^{13}C MAS experiment. Since ^{13}C−CSA tensor values also bear additional information, the experiment proved to be useful beyond the scope of providing parameters for the CODEX data evaluation.

Experimental Section

The synthesis for HBC−C_{12} and HBC−PhC_{12} was described in refs 10 and 11, respectively. The wide-angle X-ray scattering (WAXS) experiments were performed using both a $\theta-\theta$ diffractometer and a 2D X-ray detection system. The $\theta-\theta$ diffractometer (Siemens) operating in the reflection mode was used for the macroscopically unoriented material. Scattered intensity was measured in the 2θ range between 1° and 32° with 0.02° steps. Two states at 300 and 400 K were considered as representing the solid and the LC phases, respectively. For the oriented filaments, the WAXS measurements were conducted using a rotating anode (Rigaku 18 kW) X-ray beam with a pinhole collimation and a 2D detector (Siemens) with 1024 × 1024 pixels. A double graphite monochromator for the CuKα radiation (λ = 0.154 nm) was used. The beam diameter was about 0.5 mm and the sample to detector distance was 80 mm. Measurements were performed for cylindrical filaments with a thickness of about 0.7 mm. The patterns were recorded with vertical orientation of the filament axis and with the beam perpendicular to the filament. Independently of the detection system, the recorded scattered intensity distributions are presented as functions of the length of the scattering vector (s = 2 sin θ/λ, where θ is the scattering angle).

For the NMR measurements the samples were used as-synthesized, i.e., not subjected to macroscopic orientation or thermal treatment. The ^{13}C-^{1}H 2D correlation spectra and the 1D heteronuclear multiquantum filtered spectra were recorded on a Bruker DRX700 spectrometer operating at 700.13 MHz for ^{1}H and 176.05 MHz for ^{13}C with a spinning speed of 30 kHz.

Under fast magic angle spinning (MAS) the additional heating effect caused by air friction becomes significant. Using the ^{119}-Sn resonance of $Sm_2Sn_2O_7$ as a chemical shift thermometer, the temperature correction curve as a function of the bearing gas temperature was calibrated following the procedure described in ref 17. All stated temperatures were corrected by this procedure.

All CODEX experiments were performed using a Bruker DSX300 spectrometer operating at 300.23 MHz for ^{1}H and at 75.49 MHz for ^{13}C using 4 mm zirconia rotors spinning at 5−14 kHz. The ^{1}H and ^{13}C 90° pulse lengths varied between 3 and 4 μs. Ramped cross-polarization was used for the preparation of initial ^{13}C magnetization with a contact time of about 2 ms.[18] Proton dipolar decoupling at $\omega_{1H}/2\pi \approx 80$ kHz was applied during the recoupling π pulse trains and acquisition. For minimization of spectrometer drift effects the measurement was alternated between the CODEX signal and the reference signal roughly every 3 min. The last z filter was chosen to be at least 20 ms long.

The SUPER experiment[16] was performed on a Bruker DSX300 spectrometer operating at 75.49 MHz for ^{13}C using a 2.5 mm zirconia rotor spinning at 7 kHz with a scaling factor $\chi' = 0.155$ resulting in an effective spectral width of the indirect dimension of $\omega_r/\chi' = 45$ kHz, which is sufficiently large for the CSAs of the aromatic sp^2 carbons of interest. Since we were only interested in the aromatic carbons it was sufficient to record only one spectrum with the offset in the aromatic region at 128 ppm. For the ^{13}C 360° pulses the $\omega_{1,C} = 12.12\omega_r$ condition was satisfied by choosing the pulse strength to be 85 kHz. Special care has to be taken to apply sufficient heteronuclear decoupling during the ^{13}C 360° pulses. Optimum decoupling would be achieved with $\omega_{1,H}/\omega_{1,C} = 2$. The high ^{1}H power levels required to fulfill this condition can only be realized experimentally with the small coils of 2.5 mm rotors. In the experiments presented here the decoupling during the ^{13}C 360° pulses was chosen to be $\omega_{1H}/2\pi \approx 150$ kHz.

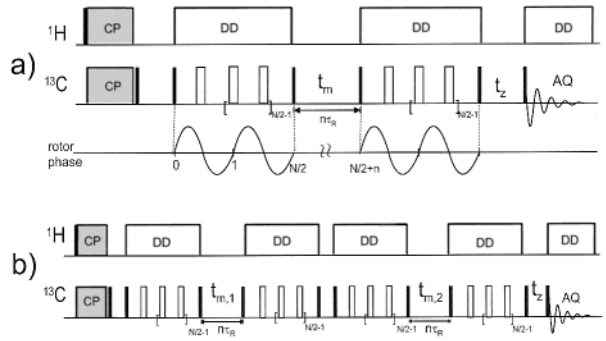

Figure 2. Pulse sequence of the CODEX (a) and the four-time CODEX (b) experiment.

Theoretical Background

In the solid state, anisotropic NMR interactions (namely, the homonuclear dipolar coupling and the chemical shift anisotropy) lead to very broad lines that obscure the chemical-shift information. The most widely used approach to overcome this problem and gain resolution is rapid sample spinning at the magic angle, MAS. If the sample is spun fast enough, anisotropic interactions are essentially averaged to zero. However, this also implies a loss of the information embodied in these anisotropic interactions. Therefore, a key principle in many solid-state NMR methods is selective recoupling of anisotropic NMR interactions by irradiation with radio frequency pulse sequences.

The CODEX experiment[14] (Figure 2a) is based on recoupling the chemical shift anisotropy by means of two identical rotor-synchronized π pulse trains. The application of such rotor-synchronized π pulse trains leads to a stimulated echo at the end of the second π pulse train. The echo signal is given as

$$S_{\text{echo}} = \left\langle \cos\frac{N}{2}\Phi_{\text{csa},1}\cos\frac{N}{2}\Phi_{\text{csa},2} + \sin\frac{N}{2}\Phi_{\text{csa},1}\sin\frac{N}{2}\Phi_{\text{csa},2} \right\rangle \quad (1)$$

where $\Phi_{\text{CSA},1}$ is the integrated phase acquired during the first π pulse train and $\Phi_{\text{CSA},2}$ the phase acquired during the second π pulse train. A full echo signal $S_{\text{echo}} = 1$ is only obtained if $\Phi_{\text{CSA},1} = \Phi_{\text{CSA},2}$. Any change of Φ_{CSA} between the two π pulse trains will lead to a characteristic signal loss. Φ_{CSA} depends on the CSA tensor orientation and on the rotor phase at the beginning of one such π pulse train.

This provides a method to probe tensor reorientations (CODEX) or to generate spinning sidebands by reconversion rotor encoding, RRE.[19] Such spinning sideband patterns can, in principle, be used to determine the chemical shift anisotropy δ and the width of the chemical shift tensor $\Delta\sigma$ as demonstrated by Hong,[20] who introduced this kind of experiment as a CSA filter. The major drawback of this method is that the asymmetry parameter η cannot be precisely determined. The SUPER experiment[16] used in this study allows the direct determination of all principal values of the ^{13}C−CSA tensor and is therefore superior to the RRE approach.

If the CODEX experiment is used for the study of slow exchange processes, the magnetization is stored on $\pm$z for a mixing time t_m, which allows time for segmental reorientation and, therefore, for a change of Φ_{CSA} leading to a signal loss characteristic for the motional process. The CODEX experiment is carried out in such a way that the mixing time is an integer multiple of the rotor period ($t_m = n\tau_r$), which is assured by a trigger. Under this condition, only molecular reorientations leading to different distinguishable CSA tensor orientations will result in a signal loss. This signal loss, compared to a reference experiment with $t_m = 0$ is the so-called pure CODEX exchange intensity

$$E(t_m, N\tau_R) = 1 - \frac{S(t_m)}{S_0(t_m = 0)} \quad (2)$$

The pure CODEX exchange intensity depends on the length of the mixing time (i.e., the correlation time of the underlying motional processes), on the overall time of anisotropic evolution $N\tau_R$, on the geometry of the motional process, and on the width $\Delta\sigma$ of the CSA tensor for nonuniaxial interactions or on the chemical shift anisotropy δ for uniaxial interactions (see ref 15).

For the determination of the correlation time the recoupling time is kept constant and the mixing time is varied. The plot of the mixing time t_m vs the pure CODEX exchange intensity E is henceforth referred to as CODEX exchange curve. By fitting this curve to a monoexponential

$$E = E_\infty\left(1 - \exp\left(-\frac{t_m}{\tau_c}\right)\right) \quad (3)$$

the correlation time τ_c of this process can be determined. The plateau value E_∞ depends on the fraction f_m of mobile segments and the number M of equivalent reorientational sites:

$$E_\infty = f_m\frac{M-1}{M} \quad (4)$$

To determine f_m and M unambiguously, the four-time CODEX experiment, which is fully described in ref 15, can be used. The four-time CODEX experiment (see Figure 2b) basically consists of two consecutive CODEX sequences. The first CODEX pulse sequence serves to select the mobile fraction. The exchange behavior of the mobile fraction is then probed by the second CODEX experiment, which is, in principle, CODEX on the mobile segments alone. For reasons of referencing, four spectra have to be recorded, which differ only in the length of the mixing times, $t_{m,1}$ and $t_{m,2}$, and the last z filter t_z. If the mixing times of the four experiments are chosen as indicated in the brackets of eq 5 (a mixing time of 0 denotes a mixing time short enough for no reorientation to occur, a mixing time of ∞ is a mixing time $t_m \gg \tau_c$) the value for $1/M$ can be determined independently of f_m by

$$\frac{1}{M} = \frac{S(0,\infty) - S(t_{m,1},\infty)}{S(0,0) - S(t_{m,1},0)} \quad (5)$$

The first mixing time $t_{m,1}$ can, in principle, be chosen freely in two of the experiments as is indicated in eq 5, but for reasons of maximal signal it is usually chosen to be well in the plateau range, i.e., $t_m \gg \tau_c$. The fraction of mobile segments f_m can subsequently be obtained from the CODEX plateau value E_∞ according to eq 4.

Variation of the overall recoupling time $N\tau_R$ while the mixing time t_m is kept constant leads to the CODEX-build-up curves. Comparison with simulated CODEX-build-up curves permits the estimation of the reorientation angle.

Results and Discussion

^{1}H-^{13}C Heteronuclear Correlation Spectra. The ^{1}H-^{1}H-DQ MAS approach used so successfully to elucidate the molecular packing in HBC−C_{12}[10] does not suffice for HBC−PhC_{12}, since the ^{1}H resonances of the aromatic protons located at the core and the phenyl ring of the side chain cannot be resolved. This

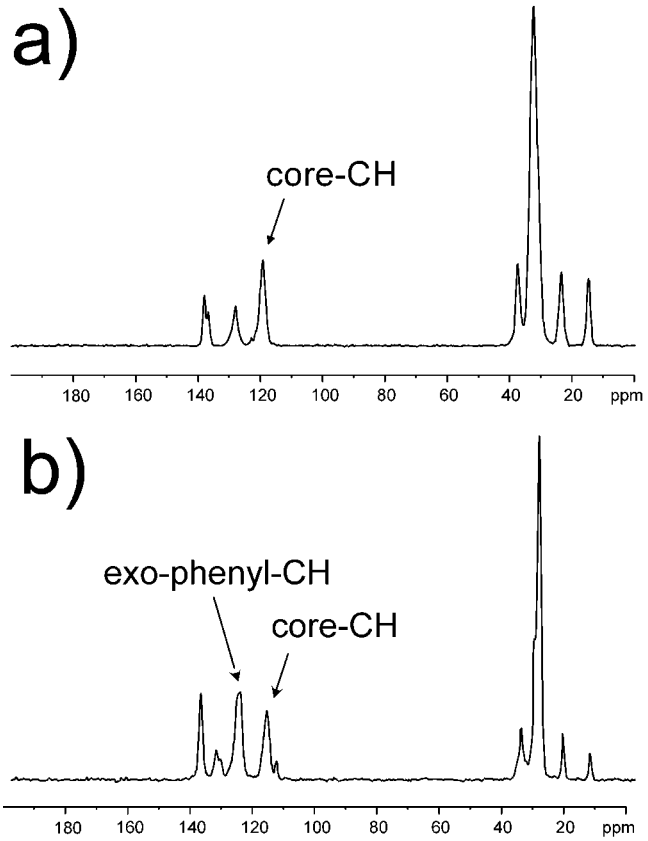

Figure 3. $^{13}C-CP$ spectra of HBC$-C_{12}$ and HBC$-PhC_{12}$ measured at 25 kHz MAS and a ^{13}C Larmor frequency of 176.05 MHz.

limitation is overcome by the ^{1}H-^{13}C-heteronuclear correlation approach, which benefits from the enhanced site-resolution of the detected ^{13}C spins and is described in refs 21 and 22. Figure 3 shows the $^{13}C-CP$ spectra of HBC$-C_{12}$ and HBC$-PhC_{12}$. Clearly, the *exo*-phenyl CH signal of HBC$-PhC_{12}$ at 130 ppm can be distinguished from the core CH signal at 120 ppm. The peak assignment was done in our previous work.[11] Figure 4 shows the ^{13}C-^{1}H heteronuclear correlation spectra for HBC$-C_{12}$ and HBC$-PhC_{12}$. The excitation time was chosen to be one rotation period and therefore almost only one-bond contacts appear as correlation peaks in the 2D spectrum.

In agreement with results from previous ^{1}H-DQ-MAS studies,[10] the heteronuclear correlation spectrum of HBC$-C_{12}$ features three distinguishable aromatic CH resonances corresponding to three different sites in the herringbone-packing arrangement. These three different sites are also observed in the simple ^{1}H spectrum, as is shown in ref 10. On the other hand, in the case of HBC$-PhC_{12}$, only two aromatic CH resonances can be distinguished, one at 130 ppm corresponding to the *exo*-phenyl CH and another at 120 ppm corresponding to the core CH. Comparison with ^{1}H chemical shifts in solution shows a π shift of around 2.5 ppm for the core protons and around 2 ppm for the *exo*-phenyl protons. This suggests that the disks in HBC$-PhC_{12}$ are also strongly interacting, but the stacking geometry differs significantly from the disk arrangement in HBC$-C_{12}$. This is also borne out by X-ray results as described in the following.

X-ray Investigations. Scattered X-ray intensity distributions recorded at two temperatures corresponding to the mesophase and to the solid state of the non oriented samples of HBC$-C_{12}$ and HBC$-PhC_{12}$ are shown in Figures 5 and 6, respectively. It is seen that the structure undergoes considerable changes upon variation of the temperature. At 130 °C, both studied materials assume comparable structures with a specific packing of columns which become locally nearly parallel and form 2D lattices in the lateral direction. The hexagonal columnar packing can be concluded at the high temperature from both the intensity distributions recorded for macroscopically isotropic samples, in which the characteristic reflections at positions 1, $\sqrt{3}$, 2 and $\sqrt{7}$ are observed, and the corresponding equatorial intensity distributions in the 2D patterns shown in Figures 7 and 8.

The parameters of the packing of columns in the two systems are different because of the differences in the side chain sizes. The lattice constants for the hexagonal packing represent the intercolumnar distances and assume values $a = 2.86$ nm and $a = 3.41$ nm for the HBC$-C_{12}$ and HBC$-PhC_{12}$ systems, respectively. These distances are the same in the macroscopically oriented and in the nonoriented samples. The vertical distances between disks in the columns also are independent of sample orientation and are $d = 0.350$ nm and $d = 0.346$ nm for HBC$-C_{12}$ and HBC$-PhC_{12}$, respectively. The patterns for the macroscopically oriented samples recorded at high temperature, Figures 7a and 8a, indicate that under these conditions the disks are perpendicular to the column axes. The strong intensity of the meridional reflections and the relatively narrow peaks observed at high temperatures for both samples can be considered an indication for an intercolumnar correlation of disk positions. The halo of intensity around the full circle is caused by the amorphous aliphatic side chains. Since the side chains are mainly located in the plane of the aromatic core, the maximum intensity is found in the meridional direction corresponding to side chain distances $d = 0.5$ nm for both HBC$-C_{12}$ and HBC$-PhC_{12}$. At the high temperature, the intensity distributions recorded for both oriented and unoriented samples are in good agreement.

Cooling to room temperature involves considerable changes in the structures of both systems. The scattered intensity distributions recorded for the two unoriented samples as well as the 2D-WAXS patterns differ significantly in the low-temperature phases of HBC$-C_{12}$ and HBC$-PhC_{12}$. There, HBC$-C_{12}$ forms a columnar phase for which the equatorial reflections can be best explained by a rectangular 2D lattice (Figure 5B) with $a = 6.1$ nm and $b = 2.38$ nm. Here, the columns are also well-aligned along the filament axis. The absence of meridional reflections in Figure 7b indicates that the disks are tilted with respect to the column axes. The estimated tilt angle is 30°, which is in nice agreement with the results from previous structure assignments utilizing a combination of NMR experimental results with quantum mechanical calculations.[13] Such a herringbone structure is the optimal arrangement for the aromatic cores and was already observed in single crystals of unsubstituted hexabenzocoronene.[23] The halo of the amorphous side chains is replaced by well-distinguishable arcs around the meridonal direction with several maxima corresponding to a better side chain order.

In the case of HBC$-PhC_{12}$ (Figure 6b), weaker structural changes are observed at the transition from the LC to the low-temperature phase. The columnar arrangement changes without remarkable changes of intracolumnar structure. Both at high and low temperatures the disks remain perpendicular to the column axes. However, a slight shift in the amorphous halo and a change of the intensity ratios of the equatorial peaks indicate density changes in the aliphatic shell. The new positions of low angle scattering peaks, which are related to the intercolumnar packing, can better be attributed to a square lattice than to a hexagonal one (Figure 6b). This is somewhat surprising, since the symmetry of a column itself is hexagonal.

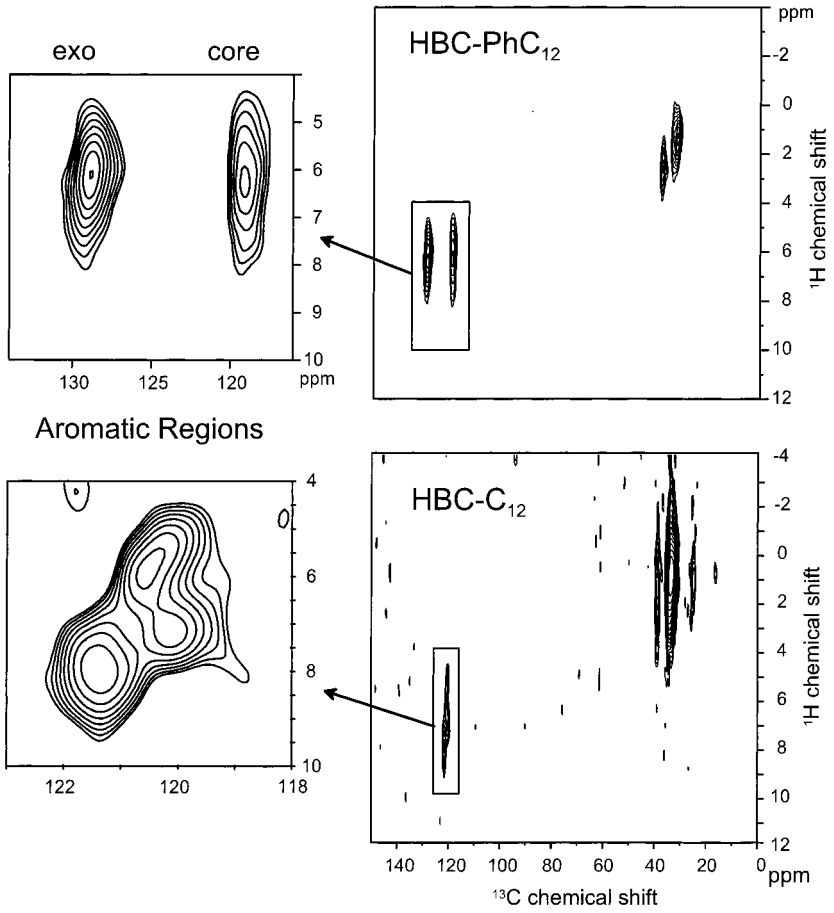

Figure 4. ^{13}C-^{1}H correlation spectra of HBC$-C_{12}$ (below) and HBC$-PhC_{12}$ (above) recorded at 30 kHz MAS with a recoupling time of $1\tau_R$.

However, this high symmetry is lost in a herringbone arrangement caused by a horizontal displacement of adjacent disks. This arrangement leads to the observed pronounced π shifts of the aromatic protons compared to the solution.[10] Since the pattern of HBC$-PhC_{12}$ shows an amorphous halo at 300K (Figure 8b), while the pattern of HBC$-C_{12}$ (Figure 7b) exhibits well-distinguishable arcs, the side chain order of HBC$-C_{12}$ is considered to be much higher than in HBC$-PhC_{12}$ under these conditions. This can also be seen in the NMR results presented below: There we show that HBC$-PhC_{12}$ has more mobile side chains at room temperature than HBC$-C_{12}$.

Dynamics in the Low-Temperature Phases. In the following we present our results on the effects of the structural differences in the low-temperature phases of HBC$-C_{12}$ and HBC$-PhC_{12}$ on the molecular dynamics. In our previous work[11] we used multiple-quantum spinning sideband patterns[21,22] to determine the dipolar coupling within the aromatic CH moieties. For the aromatic core CH groups of both HBC$-C_{12}$ and HBC$-PhC_{12}$, we found average dipolar coupling constants for a rigid, aromatic CH group in the room temperature phase. Therefore, fast column rotation as in the LC phase, which would result in a motionally reduced dipolar coupling constant, is absent.

Sideband patterns could also be obtained for the *exo*-phenyl CH group in HBC$-PhC_{12}$. By comparison with three-spin simulations of such a moiety, it is possible to draw conclusions about the dynamics of the *exo*-phenyl group. As illustrated in Figure 9, the patterns at -4 °C and 35 °C exhibit only weak third-order contributions, whereas the spectrum at -42 °C in the K_1 phase is close to a spectrum with a rigid CH group (with slightly increased first-order sidebands, possibly due to the influence of other remote protons, or a fraction of rings still performing fast motions). The experimental spectra match best with the simulations for the phenyl rings undergoing fast 180° flips around the C_2 symmetry axis. This a very common process for *para*-substituted phenyl rings.[24−27] From these data alone some ambiguity remains, since the 60° flip spectrum would also fit the experimental pattern, even though this does not appear to be a likely motional process. A distinction between both possibilities requires the application of methods probing other tensorial interactions, for instance the CSA tensor values in the phenyl group. Indeed, the quasi-static CSA powder pattern presented below (see also Figure 14) clearly corresponds to the pattern of a phenyl ring undergoing a 180° flip and not a 60° flip around its C_2 symmetry axis. Therefore, the fast 180° phenyl flip is identified as one of the dynamical processes characteristic for the intermediate solid-phase K_2 of HBC$-PhC_{12}$. In the K_1 phase at -42 °C the flip motion is essentially frozen out.

Information on the mobilities of the side chains can be retrieved from heteronuclear multiquantum (REPT-HMQ, recoupled polarization transfer-heteronuclear multiple-quantum) filtered spectra,[21,22] which are shown in Figure 10 for HBC$-C_{12}$ and HBC$-PhC_{12}$. The excitation curves, i.e., the intensity changes with increasing recoupling time, of CH_2 groups show a characteristic sharp maximum (see Figure 11). At 25 kHz MAS the signal of a rigid CH_2 group is expected to vanish completely for a recoupling time of $2\tau_R$. Thus, the mobility of a CH_2 group can be probed with this build-up behavior.

In the room-temperature spectra the signals of the α-(attached to the phenyl ring) and the (ω-1)-CH_2-group are clearly resolved. As a result of bearing air friction at these high rotor spinning speeds, the actual sample temperature for the room-temperature measurements is 35 °C. This is close to the $K_1 \rightarrow K_2$ transition temperature of HBC$-C_{12}$, and thus the observations for this sample cannot be assigned to one of these phases. The α-CH_2

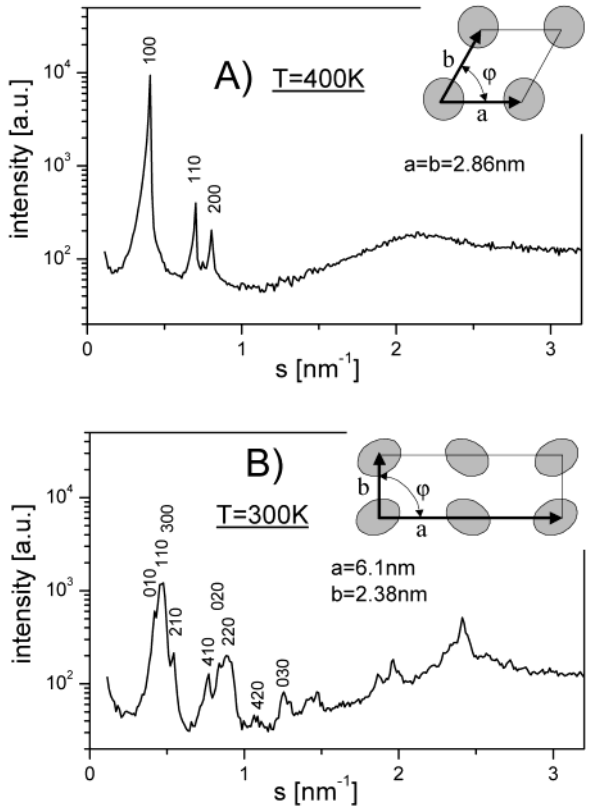

Figure 5. Scattered intensity distributions vs scattering vector for nonoriented HBC−C_{12} sample measured at (A) 400 K and (B) 300 K. The inserts indicate 2D lattices attributed to the lateral arrangement of the columns. The dominant intensity peaks are indexed as *hk*0 reflections.

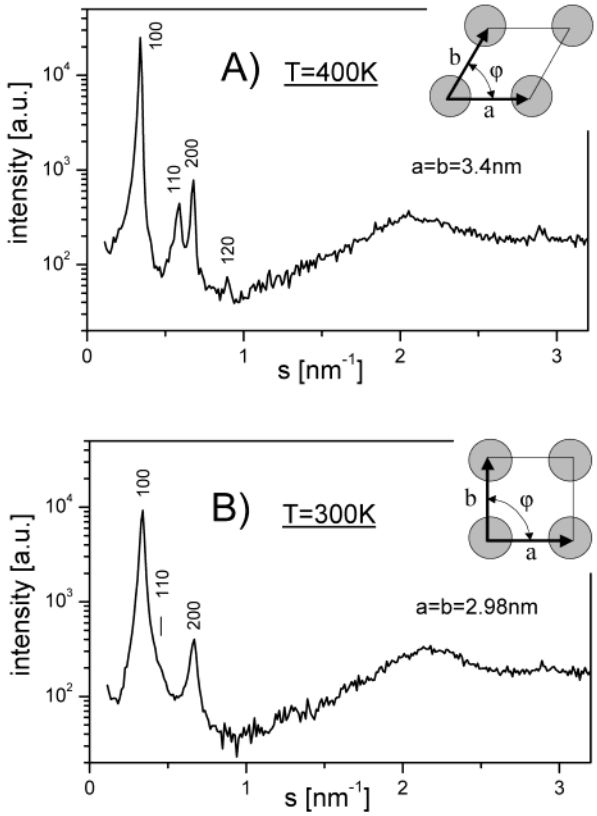

Figure 6. Scattered intensity distributions vs scattering vector for nonoriented HBC−PhC_{12} sample measured at (A) 400 K and (B) 300 K. The inserts indicate 2D lattices attributed to the lateral arrangement of the columns. The dominant intensity peaks are indexed as *hk*0 reflections.

signal of HBC−C_{12} fits nicely with the behavior of a rigid CH_2 group with signal at a recoupling time of $1\tau_r$ at 25 kHz MAS and almost no signal at $2\tau_r$. The ($\omega - 1$) signal is present in both spectra of HBC−C_{12} but does not show the "anomalous" behavior of a rigid CH_2 group. This clearly proves the existence of a mobility gradient along the chain, which is similar to the mobility gradients observed with ^{2}H NMR in a familiar triphenylene system.[28] In the case of HBC−PhC_{12} no signal is observed for the ($\omega - 1$) position at a recoupling time of $1\tau_r$ indicating more mobility in the side chains of HBC−PhC_{12}. Also the behavior of the α-CH_2 group corresponds to limited mobility of this group. This nicely agrees with the 2D-WAXS data presented above that showed much better side chain order (and therefore most probably less mobility) for HBC−C_{12}.

The measurement of rigid CH dipolar couplings as presented above does not exclude slow molecular reorientations on the second−millisecond time scale. In the following we present the results of the CODEX measurements, thus addressing such slow molecular reorientation processes: For HBC−C_{12}, CODEX measurements were carried out between −10 °C and 120 °C with mixing times varying from 100 ms to 2 s. None of these measurements resulted in pure CODEX exchange intensities significantly different from zero. In the liquid crystalline phase, the column rotation is so fast that the CODEX experiment detects only the averaged CSA tensor and, therefore, no CODEX exchange intensity is to be expected. From the line widths of the ^{1}H spectra, which do not exhibit motional narrowing, it is known that HBC−C_{12} does not undergo fast column rotation in the solid phase. The absence of pure CODEX exchange signal, therefore, proves that HBC−C_{12} does not undergo slow reorientation in the solid phase, leaving only the possibility of very slow motions. Since in the phase transition region also no pure CODEX exchange signal was detected, it must be concluded that the transition from no (or very slow and therefore nondetectable) to fast column rotation is very sharp.

In contrast, HBC−PhC_{12} disks do undergo slow reorientation in the solid phase. In the liquid crystalline phase also no pure CODEX exchange intensity was detected due to fast rotational averaging of the CSA tensor. For detailed investigation of the reorientation dynamics in the lower temperature phases of HBC−PhC_{12}, the mixing time dependencies of the pure CODEX exchange intensities were recorded for several temperatures. Figure 12 shows as an example the mixing time dependence at $T = 40$ °C for the core CH resonance at 120 ppm. The curve reaches a plateau at $E_\infty = 0.64$. Due to the symmetry of the molecule, slow in-plane 60° jumps around its C_6 symmetry axis are to be expected. In such a case the CODEX experiment cannot distinguish a 3-fold jump from a 6-fold jump due to the tensorial nature of the CSA tensor as is explained in ref 28 for the case of the quadrupole coupling. Hence, if all molecules in the sample are mobile ($f_m = 1$), a plateau value of $E_\infty = {}^2/_3 = 0.67$ is expected for six site jumps around the C_6 symmetry axis. This is in good agreement with the experimental plateau value. To justify the assumption $f_m = 1$, the number of equivalent reorientational sites M was determined unambiguously by means of the four-time CODEX experiment.

The four-time CODEX experiment requires the measurement of four spectra which differ in the length of the two mixing times $t_{m,1}$ and $t_{m,2}$. Here the spectra were measured at $T = 313$ K, $\nu_R = 10$ kHz, and dephasing and rephasing times $t_1 = t_2 = t_3 = t_4 = 7\tau_R$. The mixing times and the last z filter ($t_{m,1}$, $t_{m,2}$, and t_z) were chosen for the four experiments to be 1, 1, and 4099 ms; 2000, 1, and 2100 ms; 1, 2000, 2100 ms; and 2000, 2000, and 101 ms. After referencing the intensity to the spectrum

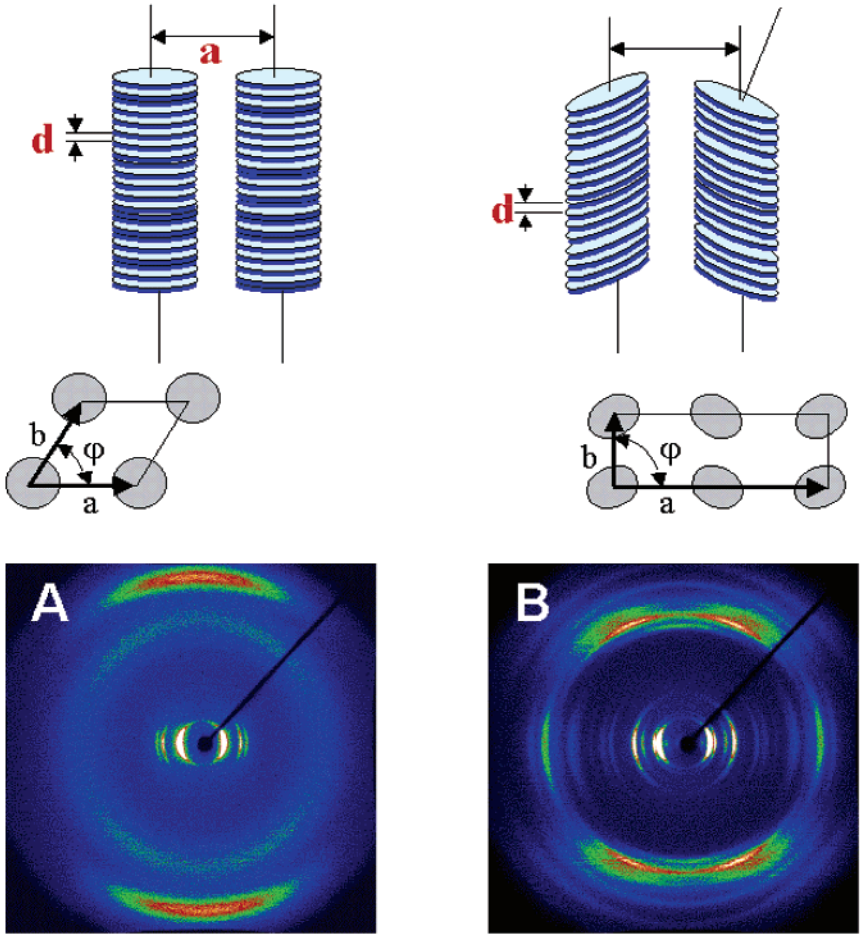

Figure 7. Two-dimensional scattering patterns for an oriented HBC−C_{12} filament as measured at (A) 400 K and (B) 300 K. The 2D lattices of intercolumnar arrangements and the orientation of disks within the columns are shown schematically.

with $t_{m,1} = t_{m,2} = 1$ ms, the value for M is obtained from the normalized signal intensities to be

$$\frac{1}{M} = \frac{E(1\text{ms},2\text{s}) - E(2\text{s},2\text{s})}{E(1\text{ms},1\text{ms}) - E(2\text{s},1\text{ms})} = \frac{0.450 - 0.254}{1 - 0.383} = 0.318 \pm 0.056 \approx \frac{1}{3}$$

for the aromatic core CH resonance at 120 ppm. This corresponds to $M =$ three equivalent reorientational sites. Hence the fraction of mobile segments is $f_m \approx 1$.

Interestingly, the mixing time dependencies of all aromatic carbon resonances of HBC−PhC_{12} are identical within the experimental errors. This clearly shows that all aromatic sites in the molecule experience the same slow molecular reorientation process. In the case of the *exo*-phenyl resonance, the CSA tensor probed by the CODEX experiment is already preaveraged by the fast phenyl flip. For the *exo*-phenyl-CH resonance the same plateau value is observed, and the number of distinguishable reorientational sites as derived from the four-time CODEX experiment is also three ($1/M = 0.293 \pm 0.038$). This has consequences for the possible average position of the phenyl ring. If the relative orientation of the phenyl ring with respect to the disk plane is retained during the disk reorientation process, the ring can only be parallel or perpendicular to the disk plane of the molecule, since otherwise six reorientational positions would be distinguishable. However, if the disk reorientation process is accompanied by a change of the relative orientation of the phenyl ring, with equal positions for opposite sites, this could again lead to the observation of only three reorientational sites of the *exo*-phenyl moiety. Therefore the average relative orientation of the *exo*-phenyl ring with respect to the disk plane remains unclear.

For the determination of the correlation time τ_c, the CODEX exchange curve was first fitted with a monoexponential given by eq 3. Since a monoexponential does not fit the experimental curve as can be seen in Figure 12, the CODEX exchange curve was fitted with a Kohlrausch−Williams−Watt (KWW) function $\exp(-t_m/\tau_{c,KWW})^{\beta})$. The β value of 0.5 indicates a broad distribution of correlation times, which can be attributed to density modulations along the column axis, originally proposed by deGennes,[29] that solve the packing problems in these materials and were indeed observed in familiar triphenylene systems.[30] Alternatively, the data can be fitted equally well with a bimodal function $E = A(1 - \exp(-t_m/\tau_{c,a})) + B(1 - \exp(-t_m/\tau_{c,b}))$ with $A + B = E_\infty$ and $\tau_{c,a} < \tau_{c,KWW} < /\tau_{c,b}$. Within experimental uncertainty, it is not possible to draw further conclusions on the correlation time distribution.

Figure 13 shows the Arrhenius plots for the rate constants derived from the KWW fit and from the bimodal fit. For the Arrhenius plot, the CODEX exchange curves at the different temperatures were constrained to a plateau value of $E_\infty = 0.67$. At lower temperatures the plateau value is not reached within reasonable mixing times. The assumption of a uniform plateau value is reasonable, if $f_m \approx 1$ is assumed for all temperatures. Rate constants were determined for a three-site jump as $k = 1/(3\tau_c)$. The apparent activation energies do not differ within the experimental errors indicating the equivalence of both fitting

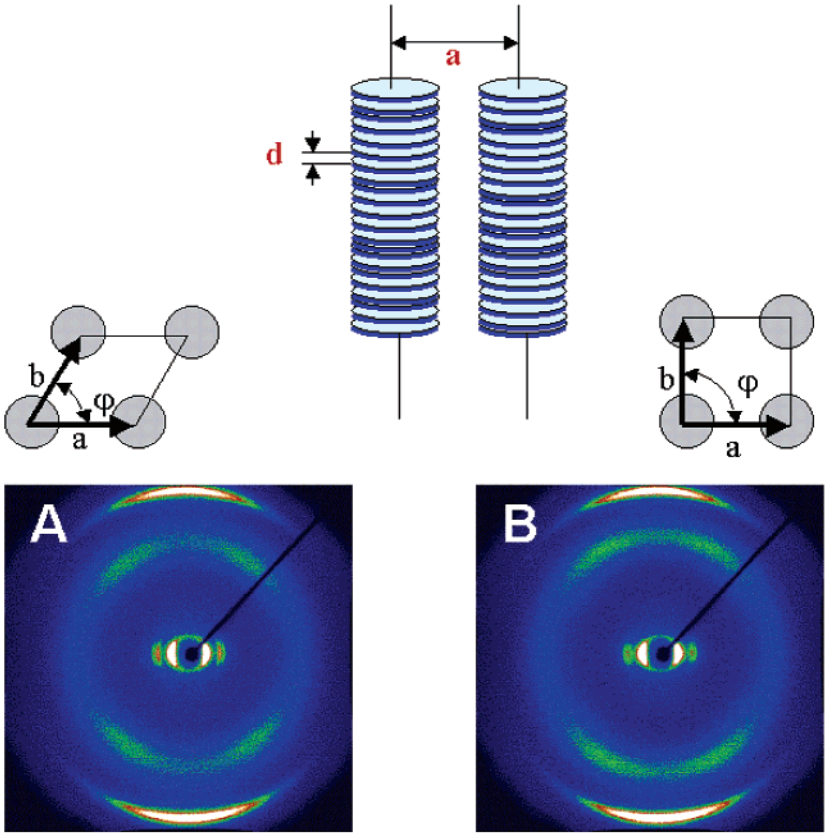

Figure 8. Two-dimensional scattering patterns for an oriented HBC−PhC_{12} filament as measured at (A) 400 K and (B) 300 K. The 2D lattices of intercolumnar arrangements and the orientation of disks within the columns are shown schematically.

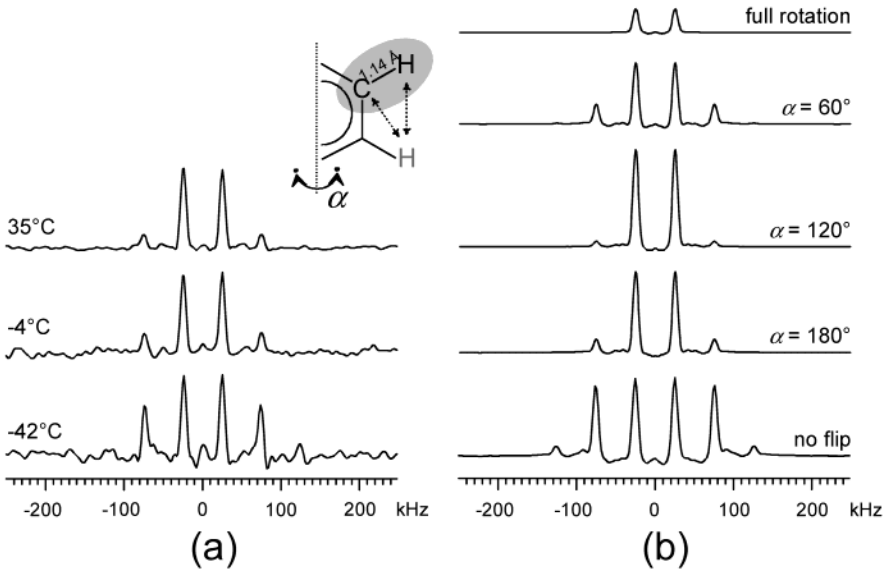

Figure 9. Experimental (a) REPT-HMQ spinning sideband patterns for the *exo*-phenyl CH signal of HBC−PhC_{12}, with $\omega_R/2\pi = 25$ kHz and a recoupling time of $2\tau_R$. Simulated spectra (b) are shown for the rigid case and for a ring performing fast flips between two sites separated by the indicated rotation angle α around the C_2 axis of the phenyl ring.

methods. It should be noted that the experimentally accessible temperature range is quite small, so the slope of the curve might only appear to be linear. The apparent activation energy derived from the KWW fits is $E_a \sim 76$ kJ/mol with a preexponential factor $k_0 = 5 \times 10^{12}$ s^{-1} for the *exo*-phenyl and $E_a \sim 59$ kJ/mol with a preexponential factor $k_0 = 8 \times 10^9$ s^{-1} for the core. Since the data are quite noisy due to the fact that they were recorded in natural abundance, the determined preexponential factors are afflicted with large errors, especially since its determination implies extrapolation over several orders of magnitude. It is therefore no surprise that the values determined here are lower than the physically reasonable values of around 10^{13} s^{-1} for a well-defined elementary jump.[31] Recently it was shown by Reichert et al.[32] that for mixing times on the time scale of seconds or longer the competing process of ^{13}C spin exchange (spin diffusion) significantly contributes to the observed CODEX signal loss. This should lead to a an increasing plateau value in the CODEX mixing time dependencies at long

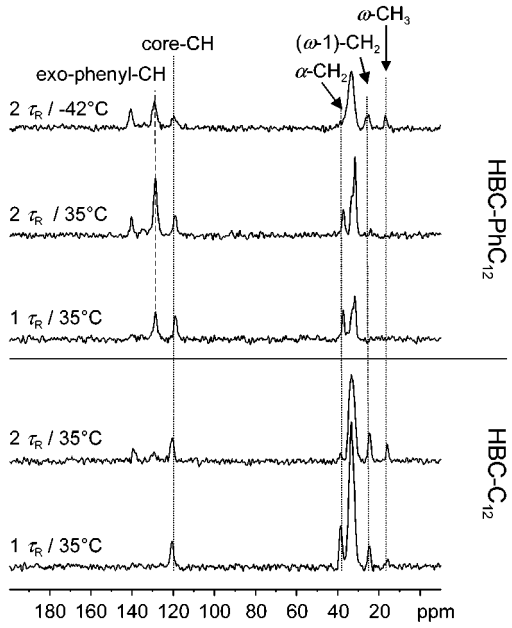

Figure 10. REPT-HMQ filtered spectra of HBC−C_{12} and HBC−PhC_{12} acquired at 25 kHz MAS. The recoupling times and temperatures are indicated on the spectra.

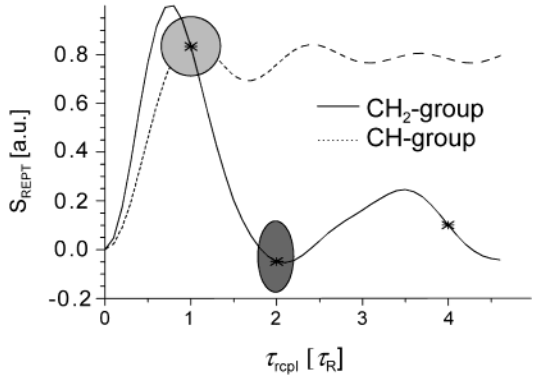

Figure 11. The expected intensity profile for a rigid CH_2 group and a C−H spin pair. Experimentally accessible points are marked as asterisks.

mixing times and could lead to a flattening of the Arrhenius plot at low temperatures, thus causing a lower apparent activation energy. The high spin diffusion constants of k_{SD} up to 0.3 s^{-1} observed in durene[33] and in a dendritic system,[34] where spin diffusion has a severe effect on the CODEX data, is for illustration indicated in Figure 13 showing that at lower temperatures a significant contribution of spin diffusion might be present. However, since we do not observe a pronounced flattening of the curve, it can be concluded that in our system spin diffusion does not have such a pronounced effect.

At temperatures above 60 °C the CODEX spectra show increasing signal loss. This is due to reorientations on the time scale of the recoupling period and a decreasing cross polarization efficiency resulting from increased molecular motion. If the correlation time is so short that significant reorientation occurs during the recoupling periods and the reference mixing time, a decrease of the plateau value is to be expected, as was shown in a model system.[36] Due to the severe signal loss at these elevated temperatures, it was not possible to observe the plateau value above 60 °C within reasonable measuring times.

To determine the reorientation angle of the motional process, CODEX build-up curves were recorded. The required ^{13}C CSA tensor values for the evaluation of the CODEX build-up curves

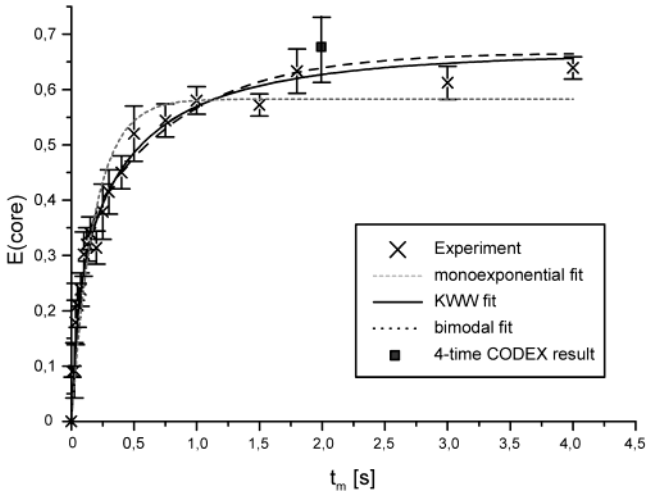

Figure 12. CODEX mixing time dependence for HBC−PhC_{12} at 42 °C for the core CH resonances. Also shown are the curves generated by the various methods of fitting and the four-time CODEX result.

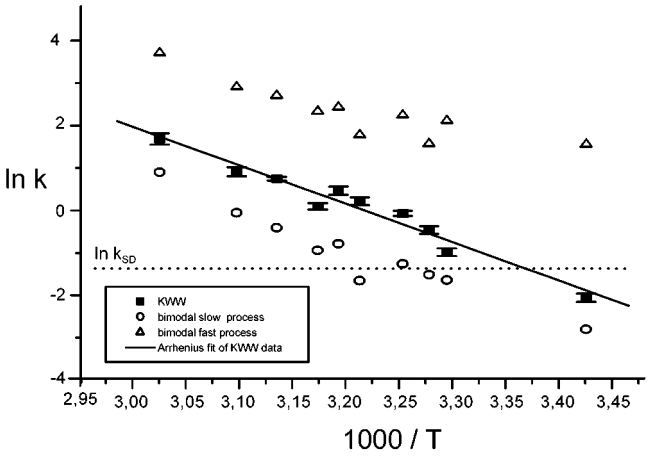

Figure 13. Arrhenius plot from the *exo*-phenyl resonance for both the rate constants derived from the KWW fits and the bimodal fits. The error bars are the errors as given by fitting routines implemented in the Microcal Origin 5.0 software package, which does not take the experimental error of each single data point into account. The real errors influenced by experimental noise are therefore bigger. The error bars for the bimodal fit exceed the plot size and are thus omitted. The reason for such large errors is that the corresponding four-parameter fit is not very stable given the accuracy of our experimental data. The dashed line indicates the spin diffusion constant observed in a dendritic system[34] as described in the text.

were determined from the quasi-static powder patterns, which are obtained as one-dimensional slices along the indirect dimension in the 2D-SUPER spectra. Figure 14 shows the powder patterns for the aromatic resonances of HBC−PhC_{12}. Since the aromatic resonances of interest were all close enough to the offset and within the spectral width in the indirect dimension, it was not necessary to subject the 2D spectrum to the shearing procedure described in ref 16 for removal of aliasing effects.

The experimental pattern of the *exo*-phenyl CH resonance (Figure 14) is clearly the pattern of a pre-averaged, almost axially symmetric aromatic ^{13}C−CSA tensor. Taking average tensor values from the literature[37] it is possible to calculate the shape of the powder patterns for different flip angles around the C_2 symmetry axis of the phenyl ring. For these calculations we used the NMR weblab software described in ref 35. As can be seen in Figure 14c the experimental pattern resembles only the pattern of the 180°-flip but definitely does not fit to a 60°

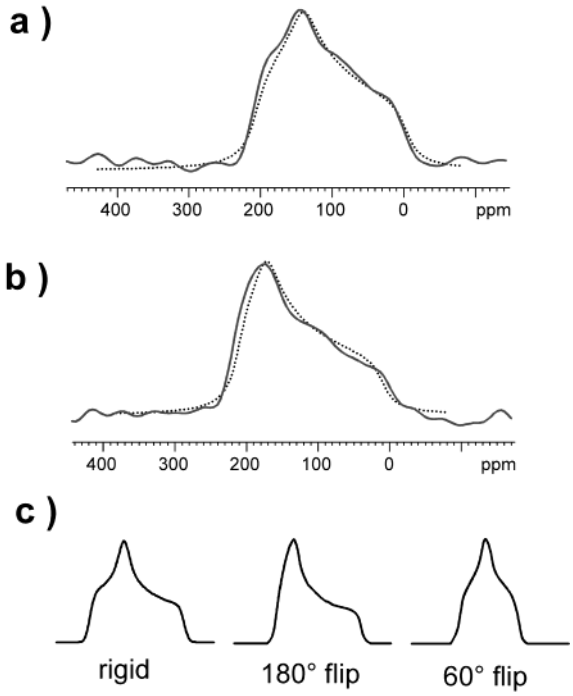

Figure 14. Quasi-static $^{13}C-CSA$ tensor patterns for the aromatic resonances of $HBC-PhC_{12}$ obtained with the SUPER experiment. (a) Experimental pattern of the core CH resonance (solid) and calculated pattern (dashed) with $\sigma_{11} = 210 \pm 5$ ppm, $\sigma_{22} = 144 \pm 3$ ppm, and $\sigma_{33} = 2 \pm 5$ ppm. (b) Experimental pattern of the *exo*-phenyl CH resonance (solid) and calculated pattern (dashed) with $\sigma_{11} = 217 \pm 10$ ppm, $\sigma_{22} = 175 \pm 3$ ppm, and $\sigma_{33} = -1 \pm 10$ ppm. (c) Schematic drawing of the powder spectrum of a rigid aromatic CH group and the powder spectra resulting from the fast averaging by a 180° and 60° flips around the C_2 symmetry axis of the phenyl ring. Since our 2.5 mm probes are not capable of measuring at temperatures necessary for freezing the ring flip, the static tensor parameters for the *exo*-phenyl CH resonance could not be determined. Therefore we calculated the schematic patterns with typical tensor values of $\sigma_{11} = 225$ ppm, $\sigma_{22} = 149$ ppm, and $\sigma_{33} = 15$ ppm, which are the average tensor values from the literature.[37]

flip. Therefore, it is proven that the fast flip motion encountered in the REPT experiments is a 180° flip around the C_2 symmetry axis of the *exo*-phenyl ring. The determination of ^{13}C chemical shift tensor values with the SUPER experiment therefore proved to be useful beyond the determination of ^{13}C tensor values alone: it can be used for the study of molecular motions and in that it is complementary to methods probing dipolar couplings, since the principal values of the CSA tensors are oriented differently in the molecular frame and are therefore averaged in another way than dipolar coupling tensors. In principle this could also serve as an alternative way for the determination of dynamic order parameters by determination of the dynamically averaged tensor values in the LC phase. However, in the case of $HBC-C_{12}$ it turned out to be difficult to obtain in the LC phase signal of the aromatic resonances after CP due to adverse $T_{1\rho}$ relaxation behavior at these temperatures.

Figure 15 shows the CODEX build-up curve at 40 °C with $t_m = 2$s and calculated curves for different reorientation angles with the tensor values determined from the quasi-static powder patterns. The experimental curve does not fit any of the simulated curves well, because it lacks the pronounced maximum. However, the initial slope fits the expected 60° jump. Some ambiguity remains, because the CODEX build-up curves are not sensitive to large reorientation angles of 60°−120°. There are several possible explanations for the missing maximum. One is the assumption of a reorientation angle distribution including small angle reorientations instead of a single sharp reorientation

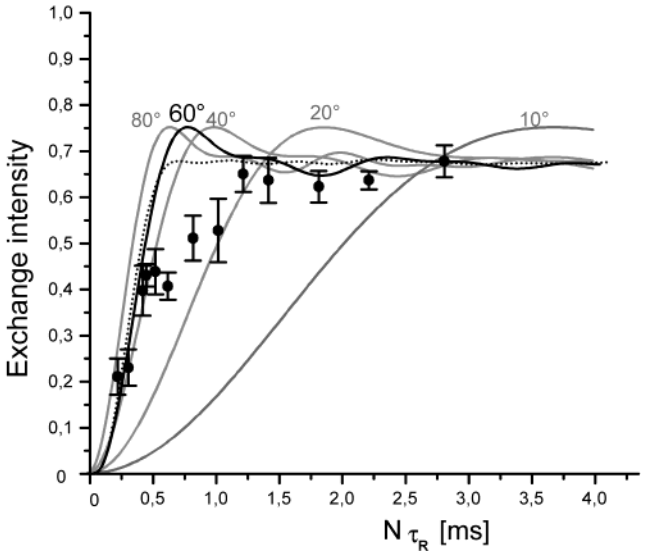

Figure 15. CODEX build-up curve for the core CH resonance of $HBC-PhC_{12}$ at $T = 40$ °C and a mixing time of 2 s. The solid lines are the curves calculated for different reorientation angles with the CSA tensor values obtained from the SUPER experiment. The dotted line was calculated with different CSAs (the σ_{zz} tensor values was arbitrarily varied by ±20 ppm for the different reorientation positions of a 60°/120° jump), and shows schematically that the pronounced maximum can be smeared out in the case of a CSA distribution.

angle. Such a reorientation angle distribution was observed in a familiar triphenylene system.[28] However, small angle contributions below 20° would lead to an increasing CODEX exchange intensity at longer recoupling times, which is inconsistent with the experimental data. Such a case was recently observed in the study of a protein hydrogel, where the missing maximum could be explained by both uniaxial rotational diffusion and random jump.[38]

Another possible explanation is the assumption of different CSA principal values for the different reorientational sites or, alternatively, different molecules. Since the slope of the CODEX build-up curve depends strongly on the width of the CSA tensor, distributions in the CSA would smear out the maximum, but leave the plateau value unchanged. This is schematically shown in Figure 15 by a curve calculated with the assumption of three different CSAs for the three reorientational positions. Even though packing effects leading to a changes in the chemical shift are not as pronounced for ^{13}C as for ^{1}H, they could still cause a shift of the isotropic chemical shift of up to 5 ppm.[39] The position of the neighboring phenyl ring could have an influence on the CSA of the core carbons. Therefore, a distribution of CSAs is also a possible explanation, if the relative position of the *exo*-phenyl ring is assumed to be varying from site to site. If this should be the case, the different orientational positions of the *exo*-phenyl rings for different sites must be unique and returned to the former orientation in case of a return jump of the disk, since otherwise the observation three distinguishable reorientational sites of the *exo*-phenyls cannot be explained.

Notwithstanding, the existence of a well-defined jump process, where the molecule returns exactly to its starting position, is supported by the observation of a constant plateau value at long recoupling times. In addition, the number of equivalent reorientational sites was determined to be three. Therefore, the dominating slow dynamical process in the solid, room-temperature phase of $HBC-PhC_{12}$ seems to be a well-defined three- (or six-) site jump around the C_6 symmetry axis of the molecule.

Conclusions

A combination of X-ray and solid-state NMR methods was successfully used for unravelling structure−property relationships in hexabenzocoronene derivatives. The differences in properties such as the intramolecular charge-carrier mobility can now be explained on the basis of differences in molecular packing and dynamics. The optimized $\pi-\pi$ packing arrangement observed in HBC−C_{12} accounts for the high charge-carrier mobility in its room-temperature phase and the prevention of slow core dynamics on the ms time-scale. The lower order of the packing in the LC phase manifests itself in a pronounced drop in the charge carrier mobility. In HBC−PhC_{12} the additional phenyl ring in the side chain prevents such optimized packing, which accounts not only for the lower charge-carrier mobility, but also for the desirable smooth charge-carrier mobility profile and the occurrence of slow reorientational dynamics. Apart from the fast ring flip of the *exo*-phenyl ring, the molecular dynamics in the room-temperature phase of HBC−PhC_{12} is dominated by well-defined 60°(or 120°) in-plane jumps of the disks.

The correlation times for this process have a broad distribution as it was found in familiar formerly investigated systems such as the various triphenylenes.[40,41] Interestingly, in an asymmetrically substituted triphenylene the onset of the axial motion of the disks around the column axes could be directly related to the glass transition.[28,42] The temperature dependence of the correlation time for this motion was found to follow the Williams−Landel−Ferry (WLF) equation.[43] It was concluded that the axial motion in the closely packed columns is a cooperative process involving several disks within the column. On the contrary, in our systems the disk rotation does not seem to be related to a glass transition. In HBC−C_{12} the disk rotation starts abruptly after the transition in the LC phase. In HBC−PhC_{12} the lower order in the room-temperature phase allows disk rotation to occur, but apparently this process is also not linked to a glass transition, although some ambiguity remains, since low temperatures were experimentally not readily accessible.

Nonetheless, we were able to establish structure property relations for HBC−PhC_{12}, a material, which has already been proven to function in a practical device[1]. In fact, the slow reorientation dynamics in the low-temperature phase of HBC−PhC_{12} reported here might improve the self-healing of the column packing, which is crucial for the long-time performance of a device.

Acknowledgment. The authors wish to thank Prof. K. Schmidt-Rohr and Dr. D. Reichert for helpful discussions and Dr. S. Brown and Dr. I. Schnell for their initial work on these systems. Finally we want to thank the BMBF "Zentrum für multifunktionelle Werkstoffe und miniaturisierte Funktionseinheiten" for financial support.

References and Notes

(1) Schmidt-Mende, L.; Fechtenkötter, A.; Müllen, K.; Moons, E.; Friend, R. H.; MacKenzie, J. D. *Science* **2001**, *293*, 1119-1122.

(2) Singh, J. *Semiconductor Optoelectronics*; McGraw-Hill: New York, 1995.

(3) Chemla, D. S.; Zyss, J. *Nonlinear Optical Properties of Organic Molecules and Crystals*; Academic Press: New York, 1987.

(4) Sage, I. C. Displays. In *Handbook of Liquid Crystals*; Demus, D., Goodby, J., Gray, G. W., Spiess, H. W., Vill, V., Eds.; Wiley-VCH: Weinheim, 1998; Vol. 1, pp 731−762.

(5) Warren, B. E. *X-ray Diffraction*; Addison Weasley: Reading, 1963.

(6) Guinier, A. *X-ray Diffraction in Crystals, Imperfect Crystals, and Amorphous Bodies*; Freeman, W. H.: San Francisco, 1963.

(7) Schmidt-Rohr, K.; Spiess, H. W. *Multidimensional Solid-State NMR and Polymers*; Academic Press: New York, 1994.

(8) Chandrasekhar, S. Columnar, Discotic Nematic and Lamellar Liquid Crystals: Their Structures and Physical Properties. In *Handbook of Liquid Crystals*, Demus, D., Goodby, J., Gray, G. W., Spiess, H. W., Vill, V., Eds.; Wiley-VCH: Weinheim, 1998; Vol. 2B, pp 749−780.

(9) Herwig, P.; Kayser, C. W.; Müllen, K.; Spiess, H. W. *Adv. Mater*. **1996**, *8*, 510-513.

(10) Brown, S. P.; Schnell, I.; Brand, J. D.; Müllen, K.; Spiess, H. W. *J. Am. Chem. Soc*. **1999**, *121*, 6712−6718.

(11) Fechtenkötter, A.; Saalwächter, K.; Harbison, M. A.; Müllen, K.; Spiess, H. W. *Angew. Chem., Int. Ed. Engl*. **1999**, *38*, 3039-3042.

(12) van de Craats, A. M.; Warman, J. M.; Fechtenkötter, A.; Brand, J. D.; Harbison, M. A.; Müllen, K. *Adv. Mater*. **1999**, *11*, 1469-1472.

(13) Ochsenfeld, C.; Brown, S. P.; Schnell, I.; Gauss, J.; Spiess, H. W. *J. Am. Chem. Soc*. **2001**, *123*, 2597−2606.

(14) deAzevedo, E. R.; Hu, W.-G.; Bonagamba, T. J.; Schmidt-Rohr, K. *J. Am. Chem. Soc*. **1999**, *121*, 8411-8412.

(15) deAzevedo, E. R.; Hu, W.-G.; Bonagamba, T. J.; Schmidt-Rohr, K. *J. Chem. Phys*. **2000**, *112*, 8988-9001.

(16) Liu, S.-F.; Mao, J.-D.; Schmidt-Rohr, K. *J. Magn. Res*. **2001**, *155*, 15−28.

(17) Langer, B.; Schnell, I.; Spiess, H. W.; Grimmer, A.-R. *J. Magn. Res*. **1999**, *138*, 182−186.

(18) Metz, G.; Wu, X.; Smith, S. O. *J. Magn. Res. A* **1994**, *110*, 219−227.

(19) Friedrich, U.; Schnell, I.; Brown, S. P.; Lupulescu, A.; Demco, D. E.; Spiess, H. W. *Mol. Phys*. **1998**, *95*, 1209−1227.

(20) Hong, M. *J. Am. Chem. Soc*. **2000**, *122*, 3762−3770.

(21) Saalwächter, K.; Graf, R.; Spiess, H. W. *J. Magn. Res*. **2001**, *148*, 398−418.

(22) Saalwächter, K.; Spiess, H. W. *J. Chem. Phys*. **2001**, *114*, 5707−5728.

(23) Goddard, R.; Haenel, M. W.; Herndon, W. C.; Krüger, C.; Zander, M. *J. Am. Chem. Soc*. **1995**, *117*, 30.

(24) Spiess, H. W. *Colloid. Polym. Sci*. **1983**, *261*, 193.

(25) Schaefer, J.; Stejskal, E. O.; McKay, R. A.; Dixon, W. T. *Macromolecules* **1984**, *17*, 1479−1489.

(26) Stumber, M.; Zimmermann, H.; Schmitt, H.; Haeberlen, U. *Mol. Phys*. **2001**, *99*, 1091−1098.

(27) Hiraoki, T.; Kogama, A.; Nishi, N.; Tsutsumi, A. *J. Mol. Struct*. **1998**, *441*, 243.

(28) Leisen, J.; Werth, M.; Böffel, C.; Spiess, H. W. *J. Chem. Phys*. **1992**, *97*, 3749−3759.

(29) deGennes, P. G. *J. Phys. Lett*. **1983**, *44*, 1−657.

(30) Werth, M.; Leisen, J.; Boeffel, C.; Dong, R. Y.; Spiess, H. W. *J. Phys. II France* **1993**, *3*, 53−67.

(31) Lausch, M.; Spiess, H. W. *Chem. Phys. Lett.* **1980**, *71*, 182−186.

(32) Reichert, D.; Bonagamba, T. J.; Schmidt-Rohr, K. *J. Magn. Res*. **2001**, *151*, 129−135.

(33) Reichert, D.; Hempel, G.; Poupko, R.; Luz, Z.; Olejniczak, Z.; Tekely, P. *Solid State Magn. Res*. **1998**, *13*, 137−148.

(34) Wind, M. Ph.D. Thesis, University of Mainz, 2001.

(35) Macho, V.; Brombacher, L.; Spiess, H. W. *Appl. Magn. Reson*. **2001**, *20*, 405−432.

(36) Saalwächter, K.; Fischbach, I. *J. Magn. Res*. **2001**. Submitted for publication.

(37) Veeman, W. S. *Prog. Nucl. Magn. Reson. Spectrosc.* **1984**, *16*, 193−235.

(38) Kennedy, S. B.; deAzevedo, E. R.; Petka, W. A.; Russell, T. P.; Tirrell, D. A.; Hong, M. *Macromolecules* **2001**, *34*, 8675−8685.

(39) Ochsenfeld, C. Private communication.

(40) Glüsen, B.; Heitz, W.; Kettner, A.; Wendorff, J. H. *Liquid Crystals* **1996**, *20*, 627−633.

(41) Werth, M.; Vallerien, S. U.; Spiess, H. W. *Liq. Cryst.* **1991**, *10*, 759−770.

(42) Vallerien, S. U.; Werth, M.; Kremer, F.; Spiess, H. W. *Liq. Cryst.* **1990**, *8*, 889−893.

(43) Williams, M.; Landel, R. F.; Ferry, J. D. *J. Am. Chem. Soc*. **1955**, *77*, 3701.